



Strain-induced permeability increase in volcanic rock

Jamie Farquharson, Michael Heap, Patrick Baud

► To cite this version:

Jamie Farquharson, Michael Heap, Patrick Baud. Strain-induced permeability increase in volcanic rock. *Geophysical Research Letters*, 2016, 43, pp.doi:10.1002/2016GL071540. hal-01473635

HAL Id: hal-01473635

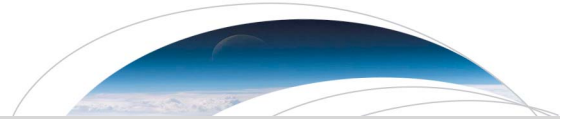
<https://hal.science/hal-01473635>

Submitted on 22 Oct 2021

HAL is a multi-disciplinary open access archive for the deposit and dissemination of scientific research documents, whether they are published or not. The documents may come from teaching and research institutions in France or abroad, or from public or private research centers.

Copyright

L'archive ouverte pluridisciplinaire **HAL**, est destinée au dépôt et à la diffusion de documents scientifiques de niveau recherche, publiés ou non, émanant des établissements d'enseignement et de recherche français ou étrangers, des laboratoires publics ou privés.



Geophysical Research Letters

RESEARCH LETTER

10.1002/2016GL071540

Key Points:

- Ascent and extrusion of lava are associated with the development of shear fractures and zones of friction-induced cataclasis
- A series of triaxial deformation experiments show that brittle failure of dense volcanic rock is accompanied by permeability increase
- Strain-induced permeability increase in the edifice may be an important mechanism for influencing pressure evolution in volcanic systems

Correspondence to:

J. I. Farquharson,
farquharson@unistra.fr

Citation:

Farquharson, J. I., M. J. Heap, and P. Baud (2016), Strain-induced permeability increase in volcanic rock, *Geophys. Res. Lett.*, 43, 11,603–11,610, doi:10.1002/2016GL071540.

Received 17 AUG 2016

Accepted 4 NOV 2016

Accepted article online 9 NOV 2016

Published online 23 NOV 2016

Strain-induced permeability increase in volcanic rock

Jamie I. Farquharson¹, Michael J. Heap¹, and Patrick Baud¹

¹Institut de Physique du Globe de Strasbourg (UMR 7516 CNRS), EOST, Université de Strasbourg, Strasbourg, France

Abstract The extrusion of dense, viscous magma typically occurs along pronounced conduit-parallel faults. To better understand the evolution of fault permeability with increasing strain, we measured the permeability of low-porosity volcanic rock samples (basalt and andesite) that were deformed in the brittle regime to various levels of inelastic strain. We observed a progressive increase in sample permeability with increasing inelastic strain (i.e., with continued sliding on the fault plane). At the maximum imposed inelastic strain (0.11), sample permeability had increased by 3 orders of magnitude or more for all sample sets. Microstructural observations show that narrow shear fractures evolve into more complex fracture systems characterized by thick zones of friction-induced cataclasis (gouge) with increasing inelastic strain. These data suggest that the permeability of conduit-parallel faults hosted in the rock at the conduit-wall rock interface will increase during lava extrusion, thus facilitating outgassing and hindering the transition to explosive behavior.

1. Introduction

Field studies show that shallow volcanic environments are riddled with fractures from the microscale to large faults and fissures, highlighting that edifice-forming material is often prone to fracture [e.g., Varley and Taran, 2003; Tuffen and Dingwell, 2005; Gaunt et al., 2014]. Spectacular manifestations of shear fracturing in volcanic environments are often observed during the emplacement of lava spines and domes: monolithic or blocky structures of dense, well-outgassed lava, which extrude along conduit-parallel faults. Notable examples include eruptive activity at Mount St Helens (Washington, USA) between 2004 and 2008, which saw the growth of a massive “whaleback” dome [Iverson et al., 2006], and the 1990–1995 eruption of Mount Unzen (Kyūshū, Japan), which culminated in the emplacement of a spine over 40 m tall [Nakada et al., 1999]. In both cases, extrusion was accompanied by large-scale cataclasis—fracturing and comminution of fragments, i.e., gouge formation—and the development of substantial shear zones at the dome/conduit margins [Smith et al., 2001; Rust et al., 2004; Iverson et al., 2006; Cashman et al., 2008; Kennedy and Russell, 2012; Hornby et al., 2015]. The thick mantle of gouge often evident during dome-building eruptive phases is testament to the significant amounts of strain, or slip, these faults have incurred [e.g., Cashman et al., 2008].

Lava domes and spines are typically extruded as part of an eruptive sequence comprising both effusive and explosive periods, and understanding how and why such transitions occur is one of the overarching goals of volcanology. It is generally understood that an efficient mechanism for outgassing magmatic gases should preclude the buildup of pore pressure in the magma, in turn reducing the explosive potential of the volcanic system. In the event that volatiles cannot escape from such a system, the prospect exists for bubble accumulation or expansion near the surface, allowing pressure augmentation within the conduit and dome and providing the kinetic energy required for explosive dome eruptions [e.g., Sparks, 1997]. Notably, observations of extruding domes highlight the common occurrence of volatile outgassing through faults and fumaroles at their margins [e.g., Johnson et al., 2008; Sahetapy-Engel and Harris, 2009; Lavallée et al., 2013]. Sparks et al. [2000] describe the appearance of gas and ash venting between the base of the dome and the neighboring wall rock at Soufrière Hills Volcano, Montserrat. Similarly, after the persistent extrusion of a dense dacitic plug between 2004 and 2005 at Mount St Helens, steaming fumaroles were recorded around its base [Pallister et al., 2013]. SO₂ emission data from Santiaguito, Guatemala, show that the volcano passively outgasses during periods of repose [Holland et al., 2011]. Peaks in the emitted volume of SO₂ are associated with explosive events involving the development of networks of shear fractures around the conduit and the generation of unconsolidated fault gouge in the shallow edifice [Holland et al., 2011; Lavallée et al., 2013]. This field evidence suggests that the ubiquity of fracture and gouge formation in the rock at the conduit-wall rock interface associated with the ascent and extrusion of viscous lava may in fact facilitate outgassing around the conduit, acting in tandem with high-temperature mechanisms at play in the conduit [e.g., Okumura et al., 2013].

Indeed, laboratory measurements by *Gaunt et al.* [2014] show that fault gouge and breccia adjacent to the Mount St Helens dome is more permeable in the direction of slip. Previous studies have explored prefailure permeability change in plutonic [Zoback and Byerlee, 1975; Kiyama et al., 1996; Mitchell and Faulkner, 2008] and volcanic [Faoro et al., 2013] rocks. In each case, a general increase in permeability is reported in the lead up to brittle failure. Despite these laboratory data, and the field evidence above, it remains unclear how permeability evolves during postfailure fault evolution in volcanic rocks. Using a suite of triaxial compression experiments, this study examines the evolution of porosity and permeability of dense volcanic rocks subject to inelastic strain, analogous to fault evolution during dome or spine formation. Armed with these experimental data, we discuss the potential for permeability evolution in the shallow conduit to influence volcanic behavior.

2. Materials and Methods

Three suites of rocks were chosen to examine the influence of progressive strain accumulation and fault development on the permeability of low- to intermediate-porosity volcanic material. The following steps (discussed in more detail below) were followed for each suite:

1. Right cylindrical cores (40 mm in length and 20 mm in diameter) were prepared from each rock type, cored parallel to each other.
2. Porosity and permeability of each cylindrical sample were measured.
3. Samples were deformed triaxially in compression to different amounts of axial strain.
4. The porosity of the deformed samples was calculated, and their permeabilities were remeasured.

The samples comprise basalt from Mount Etna (Italy), andesite collected from the El Zarco riverbed on the south-eastern flank of Volcán de Colima (Mexico), and a feldspathic andesitic lava quarried within the Kumamoto Prefecture (Japan). Nominal porosities ϕ of samples of Etna basalt (EB), El Zarco andesite (EZ), and Kumamoto andesite (KA) are 0.05, 0.08, and 0.14, respectively. Mechanical behavior of comparable samples of EB and KA has been previously studied, for example, by *Zhu et al.* [2016] and *Jeong et al.* [2007], respectively.

Porosity was determined by using helium pycnometry after vacuum-drying samples for ≥ 48 h. Gas permeability was measured by using the setup and steady state method described in *Farquharson et al.* [2016a], under a confining pressure of 1 MPa. After initial characterization, samples were soldered into copper foil jackets in order that they retained cohesion after deformation and could be subsequently recharacterized. Samples were water-saturated before being loaded into a triaxial deformation apparatus (refer to *Heap et al.* [2014a] for a schematic). During deformation we assume an effective stress law, described in terms of an effective confining pressure p_{eff} such that $p_{\text{eff}} = p_c - p_p$, where p_p is the pore pressure (distilled and deionized water). Confining pressure p_c is proportional to depth z , approximated by $p_c = \rho_b g z$, where g is acceleration due to gravity and ρ_b is the bulk density of the overlying material. We implement an effective pressure of 10 MPa, equivalent to approximately 400–500 m depth.

For each triaxial test, p_c and p_p were slowly increased to 20 and 10 MPa, respectively, achieving a p_{eff} of 10 MPa. The sample was then left overnight to allow microstructural equilibrium, whereafter the differential stress was increased at a constant strain rate (10^{-5} s^{-1}). While strain rates encountered in an active volcanic system undoubtedly vary in space and time, this value is comparable to shear rates inferred by *Rust et al.* [2003] to occur along volcanic conduit margins. Moreover, this strain rate assures that samples remain “drained” throughout deformation (deformation proceeds slower than the response of the pore pressure and the sample remains fully saturated). During all the experiments, p_c and p_p were kept constant by compensating for deviations by using servo-controlled pressure intensifiers. The recorded movement of the p_p intensifier yields the change in pore volume during nonhydrostatic deformation and unloading of the sample, which we normalize to give the porosity change $\delta\phi$, related to the volumetric strain undergone by a sample [*Baud et al.*, 2015]. We show this differential as positive during dilation and negative during compaction.

Each sample was deformed until a targeted axial strain was achieved, up to a maximum of 0.12 (i.e., a 12% reduction in sample length along the axis: the direction of the maximum principal stress). Once the targeted strain was attained, the sample was unloaded, vacuum-dried for ≥ 48 h, and its permeability was remeasured. Recent research highlights that the permeability of fractured basalt decreases with an increase in effective

Table 1. Experimental Data^a

| Sample | ϕ_0 | ε_i | $\delta\phi_i$ | ϕ_e | k_0 (m^2) | k_e (m^2) | σ_p (MPa) |
|--------|----------|-----------------|----------------|----------|------------------------|------------------------|------------------|
| EB-8 | 0.05 | 0.01 | 0.011 | 0.06 | 7.31×10^{-17} | 5.10×10^{-16} | 314.46 |
| EB-11 | 0.05 | 0.02 | 0.023 | 0.07 | 8.02×10^{-17} | 3.32×10^{-15} | 310.07 |
| EB-10 | 0.05 | 0.05 | 0.028 | 0.08 | 7.08×10^{-17} | 8.20×10^{-15} | 323.8 |
| EB-12 | 0.05 | 0.09 | 0.036 | 0.08 | 5.70×10^{-17} | 8.09×10^{-15} | 318.84 |
| EB-13 | 0.05 | 0.09 | 0.030 | 0.08 | 7.47×10^{-17} | 6.13×10^{-14} | 319.10 |
| EB-9 | 0.05 | 0.11 | 0.038 | 0.09 | 8.14×10^{-17} | 3.66×10^{-15} | 314.74 |
| EZ-2 | 0.08 | 0.00 | 0.002 | 0.08 | 2.98×10^{-16} | 2.23×10^{-15} | 215.80 |
| EZ-5 | 0.08 | 0.01 | 0.009 | 0.09 | 2.05×10^{-16} | 2.55×10^{-14} | 232.39 |
| EZ-11 | 0.07 | 0.03 | 0.016 | 0.09 | 3.08×10^{-16} | 4.29×10^{-14} | 235.21 |
| EZ-6 | 0.08 | 0.06 | 0.016 | 0.09 | 3.86×10^{-16} | 2.24×10^{-14} | 216.55 |
| EZ-7 | 0.09 | 0.07 | 0.018 | 0.11 | 5.22×10^{-16} | 9.19×10^{-14} | 174.06 |
| EZ-12 | 0.09 | 0.09 | 0.035 | 0.12 | 3.95×10^{-16} | 9.91×10^{-14} | 202.51 |
| EZ-3 | 0.07 | 0.11 | 0.026 | 0.10 | 2.97×10^{-16} | 3.36×10^{-13} | 239.07 |
| KA-2 | 0.13 | 0.01 | 0.005 | 0.14 | 1.12×10^{-16} | 4.27×10^{-17} | 140.05 |
| KA-6 | 0.15 | 0.02 | 0.007 | 0.16 | 1.11×10^{-16} | 1.21×10^{-15} | 137.66 |
| KA-4 | 0.14 | 0.03 | 0.007 | 0.15 | 1.35×10^{-16} | 5.21×10^{-15} | 133.03 |
| KA-5 | 0.15 | 0.05 | 0.015 | 0.16 | 1.32×10^{-16} | 7.25×10^{-17} | 129.58 |
| KA-9 | 0.13 | 0.11 | 0.018 | 0.14 | 7.76×10^{-17} | 9.11×10^{-14} | 142.51 |

^aEB = Etna basalt, EZ = El Zarco andesite, KA = Kumamoto andesite. ϕ_0 = initial porosity, ε_i = inelastic strain, $\delta\phi_i$ = inelastic porosity change (increase), ϕ_e = postdeformation porosity, k_0 = initial permeability, k_e = postdeformation permeability, σ_p = peak stress.

pressure [Nara et al., 2011]. Thus, permeability measured under 1 MPa will be higher than that at the in situ effective pressure (10 MPa). However, Nara et al. [2011] show that the decrease in permeability up to $p_{\text{eff}} = 10$ MPa is small. We therefore consider any difference in measured permeability across our sample suites as representative of the in situ (10 MPa) changes. In order to examine inelastic strain ε_i , we subtract the elastic strain ε_e —recovered during the unloading of the sample—from the targeted strain accumulated during the experiment (inelastic strain is thus always slightly lower than the targeted value). Similarly, in order to study the inelastic porosity change $\delta\phi_i$, we subtract the elastic porosity change—recovered during unloading—from the total porosity change measured during triaxial deformation.

3. Results

Table 1 shows the physical property data and experimental conditions for all samples. Mechanical data for each sample suite are given in Figure 1. Consistently, we observe five symptomatic stages of dilatant failure under compression [e.g., Brace et al., 1966; Hoek and Bieniawski, 1965; Kennedy and Russell., 2012], as highlighted in Figure 1a, inset: (1) the stress-strain curve is concave upward, a consequence of closure of microcracks aligned perpendicular to the direction of loading; (2) the curve is approximately linear, as the competing effects of elastic crack closure and elastic crack opening are counterbalanced; (3) the curve deviates from linear behavior as the stress is sufficient to generate new dilatant microcracks (the onset of inelastic deformation: C'); (4) the material achieves a peak stress—its compressive strength—after which failure is marked by a significant stress drop; and (5) with ongoing strain, samples exhibit a more or less constant residual stress characterized by a flattening of the respective stress-strain curves.

Inelastic change in porosity is shown in Figure 2a, as a function of inelastic strain accumulated by each sample. Samples with the lowest initial porosity (EB) undergo the greatest relative increase in porosity for a given amount of strain, whereas the most porous sample set (KA) yields the lowest relative change. Permeability is shown against inelastic strain in Figure 2b. A general increase in permeability can be observed with increasing accumulation of strain.

Figure 3 illustrates the three evolving properties—porosity, permeability, and strain—for each sample. For the lowest-porosity sample suites, EB (Figure 3a) and EZ (Figure 3b), permeability always tends to be higher than the initial value following the accumulation of inelastic strain. In detail, the permeability of EB increases from $\sim 7.29 \times 10^{-17} \text{ m}^2$ (the mean initial value of the suite) to a maximum of $6.13 \times 10^{-14} \text{ m}^2$. The mean starting permeability of EZ was $3.23 \times 10^{-16} \text{ m}^2$, which increased to $3.36 \times 10^{-13} \text{ m}^2$ after being taken to an

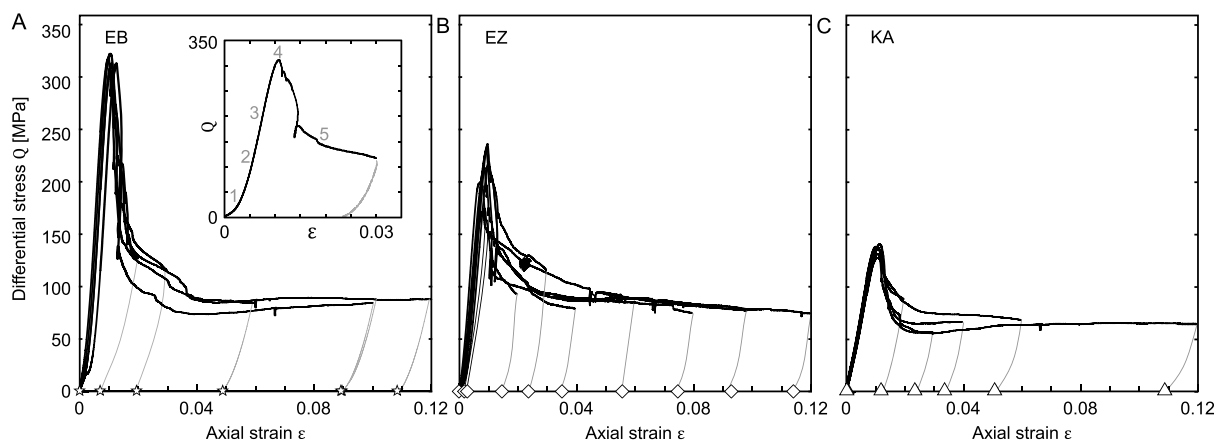


Figure 1. Mechanical data for all samples: differential stress applied to the sample versus axial strain ϵ . Symbols represent the inelastic strain accumulated (strain after unloading). (a) EB = Etna basalt. (b) EZ = El Zarco andesite. (c) KA = Kumamoto andesite. Inset: data from one experiment (EB-11), indicating different stages of deformation. Refer to text for details.

inelastic strain of 0.11. The higher-porosity KA exhibits more complex behavior: moderate decreases in permeability during some experiments and an overarching trend of increasing permeability with increasing strain. Permeability changes in KA are typically associated with little or no inelastic porosity change (Figure 3c).

4. Discussion

There is a notable influence of initial sample porosity on mechanical behavior (Figure 1): relatively low-porosity samples are stronger than their more porous counterparts, recognized by previous studies on volcanic rocks [e.g., Heap *et al.*, 2015; Schaefer *et al.*, 2015; Zhu *et al.*, 2016]. Moreover, the degree to which porosity is influenced by a given amount of strain is also dependent on the initial porosity of the rock: the lower the starting porosity, the greater the induced dilation (Figure 2). This dilation is seemingly tied to the evolution of permeability in these materials. Figure 3 shows the physical property evolution as samples are subjected to greater amounts of inelastic strain. For the two lowest-porosity sample suites, EB and EZ, these properties evolve essentially as predicted for undamaged volcanic rocks [Heap *et al.*, 2014b; Farquharson *et al.*, 2015], following a power law distribution such that $k = f\phi^m$, where m is a relatively high exponent (typically > 6) and f is a scaling prefactor. At a higher initial porosity—the Kumamoto samples—this relation is less well

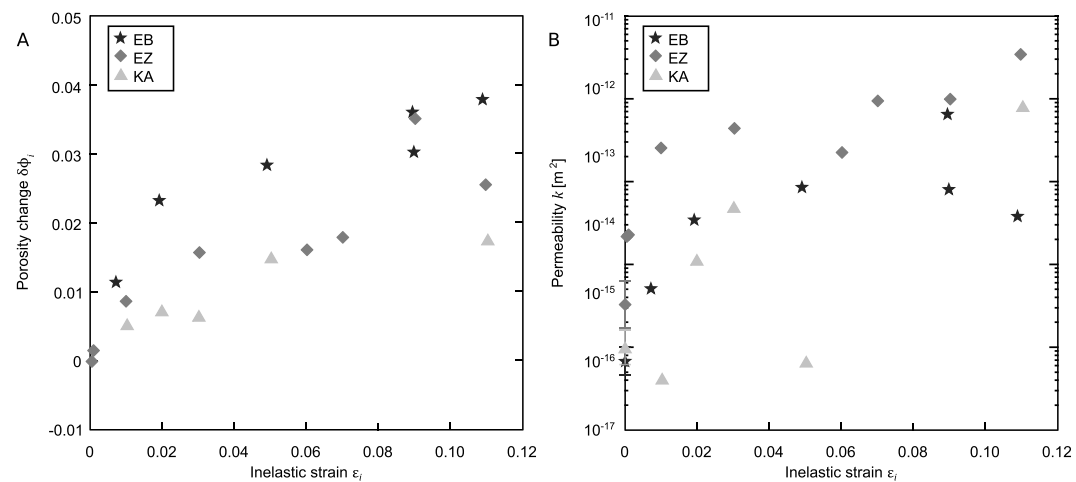


Figure 2. Change in physical properties as a function of inelastic strain. (a) Inelastic change in porosity against the inelastic strain. Positive numbers indicate dilation (porosity creation). EB = Etna basalt, EZ = El Zarco andesite, KA = Kumamoto andesite. (b) Permeability change with inelastic strain. Initial range of permeability values indicated by error bars on y axis.

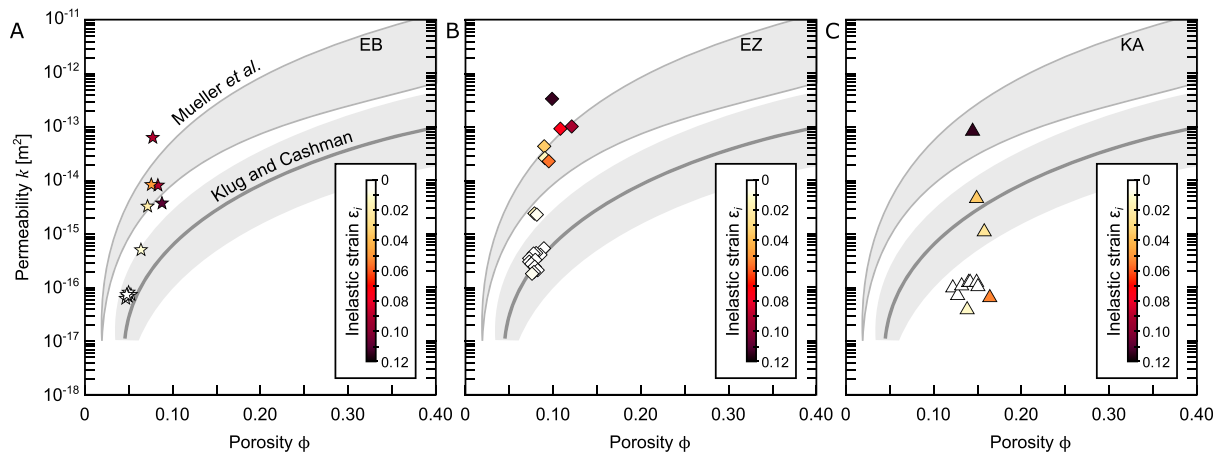


Figure 3. Permeability and porosity evolution with strain. Inelastic strain accumulated by each sample is represented by the color bar. (a) Etna basalt (EB). (b) El Zarco andesite (EZ). (c) Kumamoto andesite (KA). The shaded regions represent the permeability-porosity models of Klug and Cashman [1996] and Mueller et al. [2005] as indicated.

constrained and the data exhibit greater scatter. The fact that these data do not follow a simple power law distribution highlights that there are additional complexities to permeability evolution that are not merely a first-order function of porosity change. Nonetheless, despite small changes in porosity, we observe relatively large changes in permeability: for each sample set, deformation up to an inelastic strain of 0.11 yielded an increase in permeability of 3 orders of magnitude or greater, irrespective of the amount of dilation (Table 1 and Figure 3). Permeability-porosity models of Klug and Cashman [1996] and Mueller et al. [2005] are shown in Figures 3a–3c. Clearly, by inducing dilation through deformation, the damaged samples presented herein tend to exhibit a higher permeability than nominally undamaged volcanic rock for a given porosity.

Brittle failure in volcanic rocks is the result of propagation and coalescence of microcracks, which culminate in the generation of a macroscopic fracture through the sample. An example is shown in Figure 4a, a scanning electron microscope backscattered image of sample KA-2 after deformation up to an inelastic strain of 0.01. Figure 4a shows shear fractures oriented obliquely to the maximum principal stress (the direction of loading). Relatively little damage can be observed elsewhere in the sample. In more detail, Figure 4b highlights the coalescence of two neighboring fractures. Once this fracture plane is established, continued strain serves to increase the complexity and width of the fault through the process of cataclasis. Cataclasis is manifest in the generation of fault gouge, a friction-driven mechanism involving fracturing and comminution as well as movement and rotation of rigid fragments [e.g., Engelder, 1974]. So it is that after a greater degree of strain we observe more evolved microtextures (Figure 4c shows an image of sample KA-9, deformed to an inelastic strain of 0.11). As well as the development of macroscopic shear faults in these samples, we observe that increasing strain promotes conjugate faulting, manifest in secondary fractures which intersect the primary fault at angles of around 60° and 120° (Figure 4c). Moreover, the primary fault zone is itself relatively much wider than its low-strain counterpart (typically around a factor of 5 between the two examples KA-2 and KA-9; cf. Figures 4b and 4d). When subject to higher strains, a simple shear fracture evolves into a zone of damage, comprising pulverized material originating from either fracture plane (Figure 4d). The degree of shear is evident in the occurrence of crystal fragments entrained within the shear band, which provide natural strain markers.

From our experimental data we can infer that in shallow volcanic environments, during periods of extrusion, one should expect to observe ongoing dilation and permeability increase of several orders of magnitude as dense material within the conduit margin zone (comprising the magma at the conduit margin and the adjacent wall rock) is subject to high and persistent strains. Effective shallow-system outgassing—via strain-induced dilation—may preclude pressure buildup and facilitate effusive behavior or quiescence.

Field evidence supports the conclusion that the mechanisms of shear fracturing and friction-driven gouge generation result in increased permeability in shallow volcanic environments (i.e., under low confining pressures). For example, at Mount Unzen, the emergence of a lava dome in 1991 coincided with the

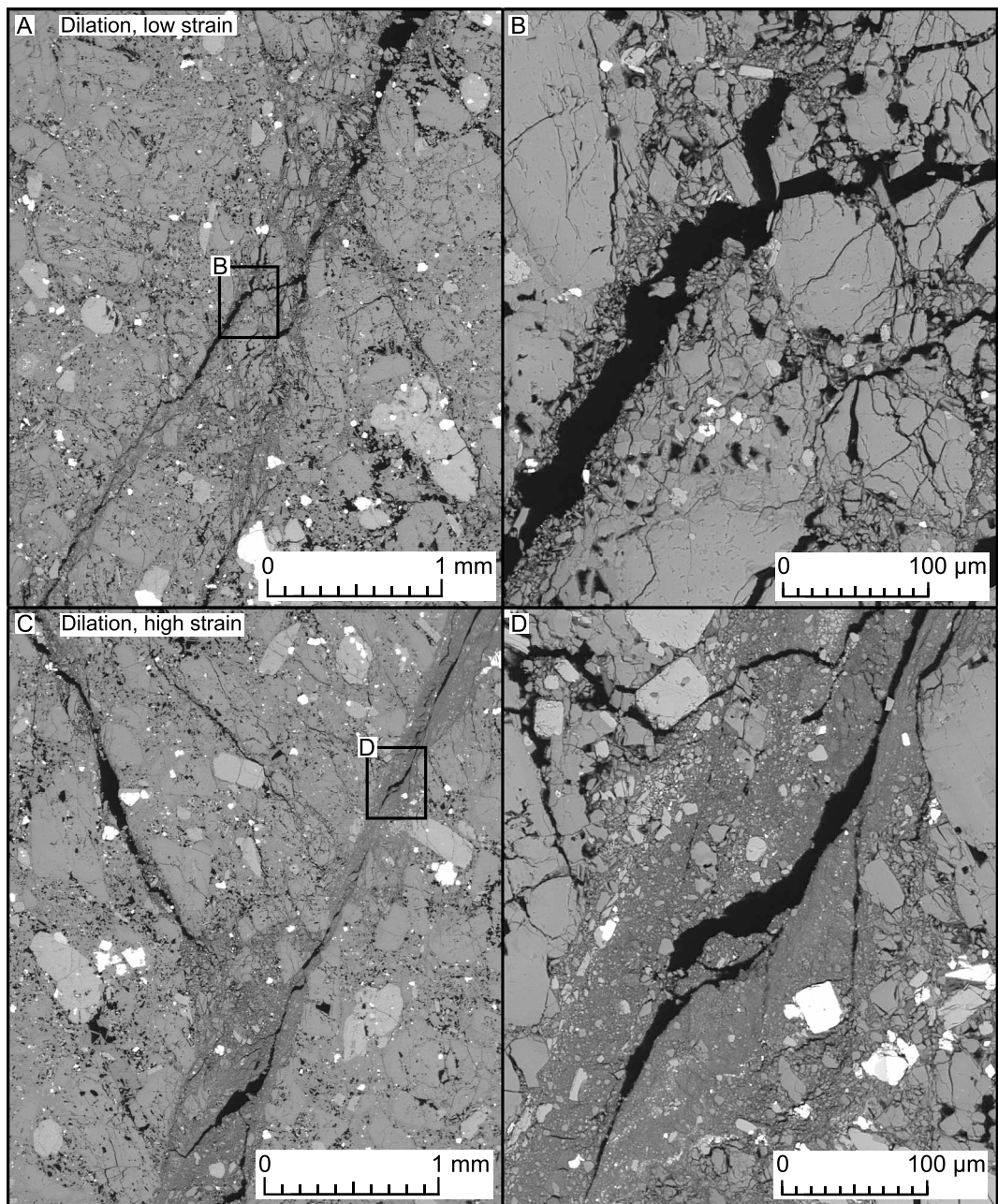


Figure 4. Evolution of damage with strain during dilation. In all cases, maximum principal stress is oriented parallel to the core axis (vertically in the images). (a) Kumamoto andesite (KA-2) deformed at $p_{\text{eff}} = 10 \text{ MPa}$ to an inelastic strain of 0.01. Coalesced cracks cut across the sample as a macroscopic fracture (porosity is black). Note that macroscopic fracture appears to have evolved stepwise, with smaller fractures being progressively interlinked by connecting cracks. (b) Detailed view of fracture shown in Figure 4a. Jigsaw-fit geometry of fracture planes, approximately 20 μm apart. Occasional granular material can also be seen on fracture margins. (c) Kumamoto andesite (KA-9) deformed at $p_{\text{eff}} = 10 \text{ MPa}$ to an inelastic strain of 0.11. As with KA-2, a macroscopic fracture can be seen through the sample. Higher strain promotes the development of a conjugate fracture system. (d) Detailed image of the interior of the fracture shown in Figure 4c. Width is typically greater than 100 μm . Comminuted granular material is abundant within the fracture, with pulverized phenocrysts highlighting shear on the fault.

commencement of detectable SO_2 emission [Hirabayashi *et al.*, 1995]. Despite the generally decreasing rate of lava extrusion between 1991 and 1994, Hirabayashi *et al.* [1995] show that the discharge rate of SO_2 over the same time period remained high (hundreds of tons per day). These authors estimate that around 80% of the potential sulfur inventory was outgassed over that time, indicating that the generation of extensive zones

of cataclasis associated with dome and spine extrusion at Mount Unzen [Smith *et al.*, 2001] constituted a highly effective outgassing mechanism: we suggest that this may have contributed to the gradual cessation of activity by 1995.

Indeed, many Vulcanian eruptive sequences comprise at least one protracted period of dome extrusion, where we would expect the development of progressively thick zones of cataclasis (e.g., Figure 4) and highly permeable fault zones around the conduit margins and in the shallow edifice (Figure 3). This is often accompanied by voluminous discharges of SO₂ after the onset of extrusive activity [e.g., Delgado-Granados *et al.*, 2001], suggesting that networks of shear fractures allow efficient outgassing to occur. Lengthening repose times between successive Vulcanian eruptions—as observed at Soufrière Hills Volcano [Herd *et al.*, 2005] and Popocatépetl, Mexico [Delgado-Granados *et al.*, 2001; De la Cruz Reyna *et al.*, 2008], for example—show that the threshold pressure required for explosive failure [e.g., Melnik and Sparks, 2002; Koyaguchi *et al.*, 2008] becomes progressively more difficult to attain [Edmonds and Herd, 2007].

We propose that strain-induced dilation of rock at the conduit-wall rock interface often accompanies the ascent and/or extrusion of viscous magma. As zones of fractures evolve as a function of increasing strain, the permeability of the shallow conduit margins increase, potentially by several orders of magnitude as suggested by our data. Consequently, magmatic volatiles may be efficiently siphoned from the system, prolonging—and eventually precluding—the generation of pore overpressures. This may be a common process that governs—to some extent—gas pressure evolution in the edifice and upper conduit, augmenting or counteracting overarching deep magmatic processes. Gas pressure increase in volcanic systems will occur if and when the influence of dilatant mechanisms—such as the one described herein—are counterpoised by permeability-reducing processes such as viscous densification [e.g., Okumura and Sasaki, 2014; Wadsworth *et al.*, 2016].

While we have focused on fractures in the shallow edifice (upper 500 m), geophysical signals that potentially signify brittle failure have been recorded at various depths in different systems. For example, Neuberg *et al.* [2006] infer fracture mechanisms operative up to 1500 m below the crater of Montserrat, while Petrosino *et al.* [2011] identify long-period seismicity—often attributed to shear fracture events—as deep as 4 km in the edifice of Volcán de Colima. Moreover, Farquharson *et al.* [2016b] show experimentally that edifice embrittlement may occur due to pore fluid migration in deep regions of the edifice. As such, the influence of strain-induced permeability increase at the conduit margin may be an important factor dictating permeability evolution in much of the edifice.

Acknowledgments

Alexandra Kushnir and Luke Griffiths are thanked for inspiring discussions. Fieldwork was funded in part by the framework of the LABEX ANR-11-LABX-0050_G-EAU-THERMIE-PROFONDE and therefore benefits from a funding from the state managed by the French National Research Agency as part of the Investments for the future program. J.I.F. acknowledges an Initiative d'Excellence (IDEX) "Contrats doctoraux" grant from the French State. M.J.H. acknowledges Initiative d'Excellence (IDEX) Attractivité grant "VOLPERM." We thank Philip Meredith and Yoshi Nara for providing samples of Etna basalt and Kumamoto andesite, respectively. We are grateful to Nick Varley and Oliver Lamb for field assistance at Volcán de Colima. We are also grateful to two anonymous reviewers, whose comments helped improve the manuscript. Data are provided in section 3, or available on request to corresponding author.

References

- Baud, P., T. Reuschlé, Y. Ji, C. S. Cheung, and T.-F. Wong (2015), Mechanical compaction and strain localization in Bleurswiller sandstone, *J. Geophys. Res. Solid Earth*, 120, 6501–6522, doi:10.1002/2015JB012192.
- Brace, W. F., B. W. Paulding, and C. H. Scholz (1966), Dilatancy in the fracture of crystalline rocks, *J. Geophys. Res.*, 71(16), 3939–3953, doi:10.1029/JZ071i016p03939.
- Cashman, K. V., C. R. Thornber, and J. S. Pallister (2008), From dome to dust: Shallow crystallization and fragmentation of conduit magma during the 2004–2006 dome extrusion of Mount St. Helens, Washington. *US Geological Survey professional paper*, (1750), pp. 387–413.
- De la Cruz-Reyna, S., I. Yokoyama, A. Martínez-Bringas, and E. Ramos (2008), Precursory seismicity of the 1994 eruption of Popocatépetl Volcano, Central Mexico, *Bull. Volcanol.*, 70(6), 753–767.
- Delgado-Granados, H., L. C. González, and N. P. Sánchez (2001), Sulfur dioxide emissions from Popocatépetl volcano (Mexico): Case study of a high-emission rate, passively degassing erupting volcano, *J. Volcanol. Geotherm. Res.*, 108(1), 107–120.
- Edmonds, M., and R. A. Herd (2007), A volcanic degassing event at the explosive-effusive transition, *Geophys. Res. Lett.*, 34, L21310, doi:10.1029/2007GL031379.
- Engelder, J. (1974), Cataclasis and the generation of fault gouge, *Geol. Soc. Am. Bull.*, 85(10), 1515–1522.
- Faoro, I., S. Vinciguerra, C. Marone, D. Elsworth, and A. Schubnel (2013), Linking permeability to crack density evolution in thermally stressed rocks under cyclic loading, *Geophys. Res. Lett.*, 40, 2590–2595, doi:10.1002/grl.50436.
- Farquharson, J., M. J. Heap, N. R. Varley, P. Baud, and T. Reuschlé (2015), Permeability and porosity relationships of edifice-forming andesites: A combined field and laboratory study, *J. Volcanol. Geotherm. Res.*, 297, 52–68.
- Farquharson, J. I., M. J. Heap, Y. Lavallée, N. R. Varley, and P. Baud (2016a), Evidence for the development of permeability anisotropy in lava domes and volcanic conduits, *J. Volcanol. Geotherm. Res.*, 323, 163–185.
- Farquharson, J., M. J. Heap, P. Baud, T. Reuschlé, and N. R. Varley (2016b), Pore pressure embrittlement in a volcanic edifice, *Bull. Volcanol.*, 78(1), 1–19.
- Gaunt, H. E., P. R. Sammonds, P. G. Meredith, R. Smith, and J. S. Pallister (2014), Pathways for degassing during the lava dome eruption of Mount St. Helens 2004–2008, *Geology*, 42(11), 947–950.
- Heap, M. J., P. Baud, P. G. Meredith, S. Vinciguerra, and T. Reuschlé (2014a), The permeability and elastic moduli of tuff from Campi Flegrei, Italy: Implications for ground deformation modelling, *Solid Earth*, 5(1), 25–44.
- Heap, M. J., Y. Lavallée, L. Petrkova, P. Baud, T. Reuschlé, N. R. Varley, and D. B. Dingwell (2014b), Microstructural controls on the physical and mechanical properties of edifice-forming andesites at Volcán de Colima, Mexico, *J. Geophys. Res. Solid Earth*, 119, 2925–2963, doi:10.1002/2013JB010521.

- Heap, M. J., J. I. Farquharson, P. Baud, Y. Lavallée, and T. Reuschlé (2015), Fracture and compaction of andesite in a volcanic edifice, *Bull. Volcanol.*, 77(6), 1–19.
- Herd, R. A., M. Edmonds, and V. A. Bass (2005), Catastrophic lava dome failure at Soufrière Hills volcano, Montserrat, 12–13 July 2003, *J. Volcanol. Geotherm. Res.*, 148(3), 234–252.
- Hirabayashi, J. I., T. Ohba, K. Nogami, and M. Yoshida (1995), Discharge rate of SO₂ from Unzen volcano, Kyushu, Japan, *Geophys. Res. Lett.*, 22(13), 1709–1712, doi:10.1029/95GL01319.
- Hoek, E., and Z. T. Bieniawski (1965), Brittle fracture propagation in rock under compression, *Int. J. Fract. Mech.*, 1(3), 137–155.
- Holland, A. P., I. M. Watson, J. C. Phillips, L. Caricchi, and M. P. Dalton (2011), Degassing processes during lava dome growth: Insights from Santiaguito lava dome, Guatemala, *J. Volcanol. Geotherm. Res.*, 202(1), 153–166.
- Hornby, A. J., et al. (2015), Spine growth and seismogenic faulting at Mt. Unzen, Japan, *J. Geophys. Res. Solid Earth*, 120, 4034–4054, doi:10.1002/2014JB011660.
- Iverson, R. M., et al. (2006), Dynamics of seismogenic volcanic extrusion at Mount St Helens in 2004–05, *Nature*, 444(7118), 439–443.
- Jeong, H. S., S. S. Kang, and Y. Obara (2007), Influence of surrounding environments and strain rates on the strength of rocks subjected to uniaxial compression, *Int. J. Rock Mech. Mining Sci.*, 44(3), 321–331.
- Johnson, J. B., J. M. Lees, A. Gerst, D. Sahagian, and N. Varley (2008), Long-period earthquakes and co-eruptive dome inflation seen with particle image velocimetry, *Nature*, 456(7220), 377–381.
- Kennedy, L. A., and J. K. Russell (2012), Cataclastic production of volcanic ash at Mount Saint Helens, *Phys. Chem. Earth Parts A/B/C*, 45, 40–49.
- Kiyama, T., H. Kita, Y. Ishijima, T. Yanagidani, K. Aoki, and T. Sato (1996), Permeability in anisotropic granite under hydrostatic compression and triaxial compression including post-failure region, in *2nd North American Rock Mechanics Symposium*, American Rock Mechanics Association, Montréal, Canada.
- Klug, C., and K. V. Cashman (1996), Permeability development in vesiculating magmas: Implications for fragmentation, *Bull. Volcanol.*, 58(2–3), 87–100.
- Koyaguchi, T., B. Scheu, N. K. Mitani, and O. Melnik (2008), A fragmentation criterion for highly viscous bubbly magmas estimated from shock tube experiments, *J. Volcanol. Geotherm. Res.*, 178(1), 58–71.
- Lavallée, Y., P. M. Benson, M. J. Heap, K. U. Hess, A. Flaws, B. Schillinger, P. G. Meredith, and D. B. Dingwell (2013), Reconstructing magma failure and the degassing network of dome-building eruptions, *Geology*, 41(4), 515–518.
- Melnik, O., and R. S. J. Sparks (2002), Modelling of conduit flow dynamics during explosive activity at Soufrière Hills Volcano, Montserrat, *Geol. Soc. London Mem.*, 21(1), 307–317.
- Mitchell, T. M., and D. R. Faulkner (2008), Experimental measurements of permeability evolution during triaxial compression of initially intact crystalline rocks and implications for fluid flow in fault zones, *J. Geophys. Res.*, 113, B11412, doi:10.1029/2008JB005588.
- Mueller, S., O. Melnik, O. Spieler, B. Scheu, and D. B. Dingwell (2005), Permeability and degassing of dome lavas undergoing rapid decompression: An experimental determination, *Bull. Volcanol.*, 67(6), 526–538.
- Nakada, S., H. Shimizu, and K. Ohta (1999), Overview of the 1990–1995 eruption at Unzen Volcano, *J. Volcanol. Geotherm. Res.*, 89(1), 1–22.
- Nara, Y., P. G. Meredith, T. Yoneda, and K. Kaneko (2011), Influence of macro-fractures and micro-fractures on permeability and elastic wave velocities in basalt at elevated pressure, *Tectonophysics*, 503(1), 52–59.
- Neuberg, J. W., H. Tuffen, L. Collier, D. Green, T. Powell, and D. Dingwell (2006), The trigger mechanism of low-frequency earthquakes on Montserrat, *J. Volcanol. Geotherm. Res.*, 153(1), 37–50.
- Okumura, S., and O. Sasaki (2014), Permeability reduction of fractured rhyolite in volcanic conduits and its control on eruption cyclicity, *Geology*, 42(10), 843–846.
- Okumura, S., M. Nakamura, K. Uesugi, T. Nakano, and T. Fujioka (2013), Coupled effect of magma degassing and rheology on silicic volcanism, *Earth Planet. Sci. Lett.*, 362, 163–170.
- Pallister, J. S., K. V. Cashman, J. T. Hagstrum, N. M. Beeler, S. C. Moran, and R. P. Denlinger (2013), Faulting within the Mount St. Helens conduit and implications for volcanic earthquakes, *Geol. Soc. Am. Bull.*, 125(3–4), 359–376.
- Petrosino, S., P. Cusano, M. La Rocca, D. Galluzzo, J. Orozco-Rojas, M. Bretón, J. Ibáñez, and E. Del Pezzo (2011), Source location of long period seismicity at Volcán de Colima, México, *Bull. Volcanol.*, 73(7), 887–898.
- Rust, A. C., M. Manga, and K. V. Cashman (2003), Determining flow type, shear rate and shear stress in magmas from bubble shapes and orientations, *J. Volcanol. Geotherm. Res.*, 122(1), 111–132.
- Rust, A. C., K. V. Cashman, and P. J. Wallace (2004), Magma degassing buffered by vapor flow through brecciated conduit margins, *Geology*, 32(4), 349–352.
- Sahetapy-Engel, S. T., and A. J. Harris (2009), Thermal structure and heat loss at the summit crater of an active lava dome, *Bull. Volcanol.*, 71(1), 15–28.
- Schaefer, L. N., J. E. Kendrick, T. Oommen, Y. Lavallée, and G. Chigna (2015), Geomechanical rock properties of a basaltic volcano, *Front. Earth Sci.*, 3, 1–15.
- Smith, J. V., Y. Miyake, and T. Oikawa (2001), Interpretation of porosity in dacite lava domes as ductile–brittle failure textures, *J. Volcanol. Geotherm. Res.*, 112(1), 25–35.
- Sparks, R. S. J. (1997), Causes and consequences of pressurisation in lava dome eruptions, *Earth Planet. Sci. Lett.*, 150(3), 177–189.
- Sparks, R. S. J., M. D. Murphy, A. M. Lejeune, R. B. Watts, J. Barclay, and S. R. Young (2000), Control on the emplacement of the andesite lava dome of the Soufrière Hills volcano, Montserrat by degassing-induced crystallization, *Terra Nova*, 12(1), 14–20.
- Tuffen, H., and D. Dingwell (2005), Fault textures in volcanic conduits: Evidence for seismic trigger mechanisms during silicic eruptions, *Bull. Volcanol.*, 67(4), 370–387.
- Varley, N. R., and Y. Taran (2003), Degassing processes of Popocatépetl and Volcán de Colima, Mexico, *Geol. Soc. London Spec. Publ.*, 213(1), 263–280.
- Wadsworth, F. B., J. Vasseur, E. W. Llewellyn, J. Schauroth, K. J. Dobson, B. Scheu, and D. B. Dingwell (2016), Sintering of viscous droplets under surface tension, *Proc. R. Soc. A*, 472(2188), 20150780, doi:10.1098/rspa.2015.0780.
- Zhu, W., P. Baud, S. Vinciguerra, and T. F. Wong (2016), Micromechanics of brittle faulting and cataclastic flow in Mount Etna basalt, *J. Geophys. Res. Solid Earth*, 121, 4268–4289, doi:10.1002/2016JB012826.
- Zoback, M. D., and J. D. Byerlee (1975), The effect of microcrack dilatancy on the permeability of Westerly granite, *J. Geophys. Res.*, 80(5), 752–755, doi:10.1029/JB080i005p00752.